Na *AAPPS Bulletin* (2023) 33:28
https://doi.org/10.1007/s43673-023-00103-5

AAPPS Bulletin

REVIEW ARTICLE

Open Access

Advanced operation modes relying on core plasma turbulence stabilization in tokamak fusion devices

Yong-Su Na[1*]

Abstract

Recent progress of advanced operation modes in tokamaks is addressed focusing upon internal transport barrier (ITB) discharges. These ITB discharges are being considered as one of candidate operation modes in fusion reactors. Here, "internal" means core region of a fusion plasma, and "transport barrier" implies bifurcation of transport phenomena due to suppressing plasma turbulence. Although ITB discharges have been developed since the mid-1990, they have been suffering from harmful plasma instabilities, impurity accumulation, difficulty of feedback control of kinetic plasma profiles such as pressure or current density, and so on. Sustainment of these discharges in long-pulse operations above wall saturation time is another huddle. Recent advances in ITB experiments to overcome the difficulties of ITB discharges are addressed for high β_p plasmas in DIII-D, broad ITB without internal kink mode in HL-2A, F-ATB (fast ion-induced anomalous transport barrier) in ASDEX upgrade, ion and electron ITB in LHD, and FIRE (fast ion regulated enhancement) mode in KSTAR. The core-edge integration is discussed in the ITB discharges. The DIII-D high β_p plasmas facilitate divertor detachment which weakens the edge transport barrier (ETB) but extends the ITB radius resulting in a net gain in energy confinement. Double transport barriers were observed in KSTAR without edge localized mode (ELM). FIRE modes in KSTAR are equipped with the I-mode-like edge which prevents the ELM burst and raise the fusion performance together with ITB. Finally, long sustainment of ITBs is discussed. EAST established electron ITB mode in long-pulse operations. JET achieved quasi-stationary ITB with active control of the pressure profile. JT-60U obtained 28 s of high β_p hybrid mode, and KSTAR sustained stable ITB in conventional ITB mode as well as FIRE mode. These recent outstanding achievements can promise ITB scenarios as a strong candidate for fusion reactors.

1 Introduction

The goal of tokamak plasma research for fusion is to achieve (i) high fusion performance, (ii) steady-state operation, and (iii) long-pulse operation. Regarding high fusion performance, the so-called triple fusion product, $n\tau_E T$ needs to be high enough to have positive net energy or high fusion energy gain in a reactor, where n is the plasma density, τ_E is the plasma energy confinement time, and T is the plasma temperature. The energy confinement time is a measure of the rate at which the confined plasma loses energy to its environment, defined as a ratio of the global plasma energy content to the applied total heating power in a steady condition. The normalized plasma beta (β_N) and energy confinement enhancement factor (H_{98}) are widely being used as figures of merit for fusion performance, where β_N is the normalized ratio of the plasma pressure to the magnetic pressure, $\beta_N = \beta_t \cdot a \cdot B_t / I_p$, and H_{98} is the ratio of the energy confinement time to the type-I ELMy H-mode confinement time, $H_{98} = \tau_E / \tau_{E,98}$. Here, β_t is the toroidal beta, ratio of the plasma pressure (<p>) to the toroidal magnetic pressure ($B_t^2/2\mu_0$), a is the minor radius of the plasma, B_t is the toroidal magnetic field

*Correspondence:
Yong-Su Na
ysna@snu.ac.kr
[1] Department of Nuclear Engineering, Seoul National University, Seoul, Korea

strength, and I_p is the plasma current. In terms of steady-state operation, the plasma current, which is required to confine plasmas by generating a magnetic field in poloidal direction, needs to be driven non-inductively rather than the inductive way in a tokamak. To obtain full non-inductive current drive condition ($f_{NI} = 1$), the fraction of the self-generated plasma current (f_{BS}), the so-called bootstrap current, should be high, where f_{NI} is the non-inductive current drive fraction. As f_{BS} is a function of poloidal beta (β_p), β_p is a figure of merit for steady-state operation. Lastly, regarding long-pulse operation, the pulse length needs to be longer than the wall saturation time at least, where the wall saturation time (τ_W) implies the characteristic time of the saturation of the plasma-wall interactions, typically order of hundred seconds depending on machines. The long-pulse operation encompasses engineering as well as physics demands such as plasma kinetic profile control, magnetohydrodynamic (MHD) instability control, and particle and heat exhaust. Here, τ_{pulse}/τ_W can be used as a figure of merit for long-pulse operation, where τ_{pulse} is the discharge pulse length.

Various operation scenarios have been developed in a tokamak to achieve above requirements. Here, the operation scenario implies a sequence of actions making a plasma discharge to achieve the goal.

A typical operation scenario is H-mode, being widely used in a tokamak. It is considered as the reference scenario to produce a fusion power of 500 MW with a fusion gain $Q = 10$ (that is, a fusion power ten times higher than the input heating power) in the International Thermonuclear Experimental Reactor (ITER) [1]. H-mode was discovered in 1982 in ASDEX tokamak which exhibited about twice higher particle and energy confinement time over L-mode [2]. The energy confinement enhancement factor, H_{98}, is based on the energy confinement time of H-modes so H_{98} in H-mode plasmas is usually defined to be unity. Core plasmas are believed to be mostly governed by ion temperature gradient (ITG) mode and trapped electron mode (TEM) in H-modes. The naturally peaked current density profile and accordingly monotonically increasing safety factor (q) and positive magnetic shear (s) profile from the center to the edge region of the plasma contribute this. Here, the safety factor is defined as the number of toroidal orbits per poloidal orbit, $q = \mathrm{rB_p/RB_t}$, for a circular shape plasma and the magnetic shear as the change in the pitch angle of a magnetic field line in radius, $s = \mathrm{r/q(dr/dq)}$. The MHD stability is strongly linked with the q-profile. As the central q-value is below unity, the sawtooth instability usually presents in H-mode plasmas which can trigger neoclassical tearing mode (NTM) at $q = 3/2$ or 2 surfaces, generally. Particularly, the NTM at $q = 2$ surface can significantly degrade the confinement and limit the achievable β_N. It can often result in plasma disruptions, a rapid collapse of the plasma energy. Therefore, β_N is limited below 2.0 in H-more reference scenario in ITER. H-mode plasmas are equipped with ETB due to stabilization of turbulence in the edge region. As a result, plasma pressure gets steepened which results in a local pressure- and current-driven instability, the so-called ELMs. ELMs extract plasma particle and energy confined in the ETB region to the wall surrounding the plasma periodically which ends up with severe damage of the plasma surrounding materials. Thus, ELM suppression or avoidance is required for a fusion reactor. The high-pressure gradient in the ETB region increases bootstrap current contributing to increase f_{NI} since the bootstrap current is proportional to the pressure gradient. However, f_{BS} is not that high, and f_{NI} is usually below 0.5, implying steady-state operations are not feasible in standard H-modes.

To overcome such limitations of H-modes, advanced operation scenarios have been explored [3]. They were mostly established by playing with the shape of the q-profile. ITB discharges have been developed as one of these advanced scenarios. They rely on turbulence stabilization in the core region of the plasma on the contrary to ETB. Depending on the gradient of ITB, MHD instabilities can limit achievable β_N. But owing to presence of a steep gradient region within an ITB, the bootstrap current fraction is usually large, if the ITB is not located too far inside the plasma. By reducing the plasma current in ITB scenarios compared with other scenarios, β_p can be increased which results in increase of f_{BS} as well. ITB is coined from JT-60 U [4], and it has been developed in various devices such as Alcator C-Mod [5, 6], ASDEX Upgrade [7, 8], DIII-D [9], EAST [10], HL-2A [11], JET [12], JT-60U [4, 13], KSTAR [14, 15], TFTR [16], and Tore Supra [17]. ITB shows an outstanding feature of bifurcation of the flux-gradient relationship. In other words, if ITB is formed in the energy channel, the ion or electron heat flux divided by the density does not increase over the linear relation, while the gradient of the ion or electron temperature increases [18]. The ITB can be characterized as below.

For an ITB in an energy channel, if the normalized inverse gradient length ($\mathrm{R/L_T}$) is large or small, the ITB is called as strong or weak as shown in Fig. 1, where $L_T = -\mathrm{T}/\nabla\mathrm{T}$. If ρ_{ITB} is large or small, the ITB is called as large or small, where $\rho_{ITB} = (\rho_{shoulder}+\rho_{foot})/2$, $\rho_{ITB,}$ $\rho_{shoulder}$, and ρ_{foot} are the location of the ITB, ITB shoulder, and ITB foot, respectively. ρ_{foot} can be determined by $\boldsymbol{\partial\chi/(\partial(-\nabla T))} < 0$ or maximum value of the second derivative of the profile, where $\boldsymbol{\chi}$ is the heat diffusivity. If W/a is large or small, the ITB is called as wide or narrow, where $W = \rho_{foot}\text{-}\rho_{shoulder}$ is the ITB width.

The ITB can be identified in various ways. First and most importantly, the bifurcation can be observed in

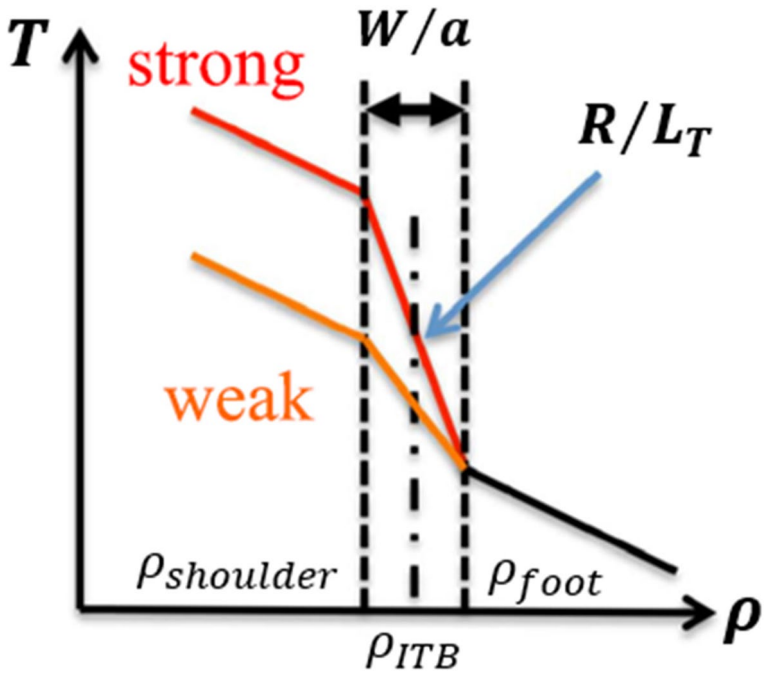

Fig. 1 Characterization of an ITB in energy transport channel

the flux-gradient relation. Second, the diffusivity drops close to the neoclassical level as the contribution from turbulence is severely reduced. Third, the normalized inverse gradient length becomes higher than the critical value set by micro-instabilities. Fourth, the measured fluctuation is reduced in the experiment and so on.

2 Recent advances in ITB experiments

Since early experiments were performed in JET, DIII-D, JT-60U, and TFTR in the mid-1990, ITB discharges have been explored in many devices to overcome their major shortcomings of low stability, impurity accumulation, short pulse-length, etc. However, it was extremely challenging so the attention to ITB scenario development was diminished to draw and moved to other advanced scenarios which require minimal feedback control such as hybrid scenarios. It is noteworthy that some hybrid scenarios also exhibit weak ITBs such as those in JT-60U which will be discussed later in this paper. However, there have been significant progress that has been made in ITB experiments recently which are highlighted here.

2.1 High β_p plasmas in DIII-D

High β_p plasmas have been established in DIII-D achieving high confinement, high stability, high normalized density (f_{GW}), and low impurity accumulation, simultaneously [19]. The high β_p regime was originally proposed for a steady-state fusion pilot plant with high f_{BS} in the 1990s [20]. Since then, a lot of progress have been made in theoretical, modeling, and experimental research activities on this topic in DIII-D. Figure 2 shows an example of high β_p discharge [19].

In this discharge (shot 154406), the plasma current is about 0.6 MA, and the steady-state condition was achieved in 3.0–7.0 s as indicated with zero surface loop voltage in Fig. 2. High beta values of β_p~3 and β_N~3 were obtained as well as high confinement enhancement factors of $H_{98} \geq 1.5$ and $H_{89} \geq 2.0$. The neutral beam injection (NBI) and electron cyclotron current drive (ECCD) were used with the power of ~7.5 MW and ~2.5 MW, respectively. As shown in kinetic profiles in Fig. 2, ITBs exist in the particle and momentum channel as well as the ion and electron energy channel. It is large ITBs with the ITB location around ρ~0.7. The minimum q-value, q_{min}, is > 2.0 with q_{95} ~7.0–12.0, where q_{95} is the q-value at 95% of the last closed flux surface. It is noteworthy that q_{95} in ITER steady-state scenario is 5.0. The Greenwald density fraction is f_{GW}~1.0–1.1, and the NBI torque was low < 2 Nm, so the high performance could be obtained and sustained even with a low toroidal rotation, consequently relatively low ω_{ExB}, which is known to play a critical role to stabilize turbulence. Transport modeling with TGYRO [21] employing TGLF [22] and NEO [23] for turbulence and neoclassical transport, respectively, confirmed that the ω_{ExB} effect is not notable [24]. As shown in the current density profiles in Fig. 2, the bootstrap current dominates around the ITB region and in

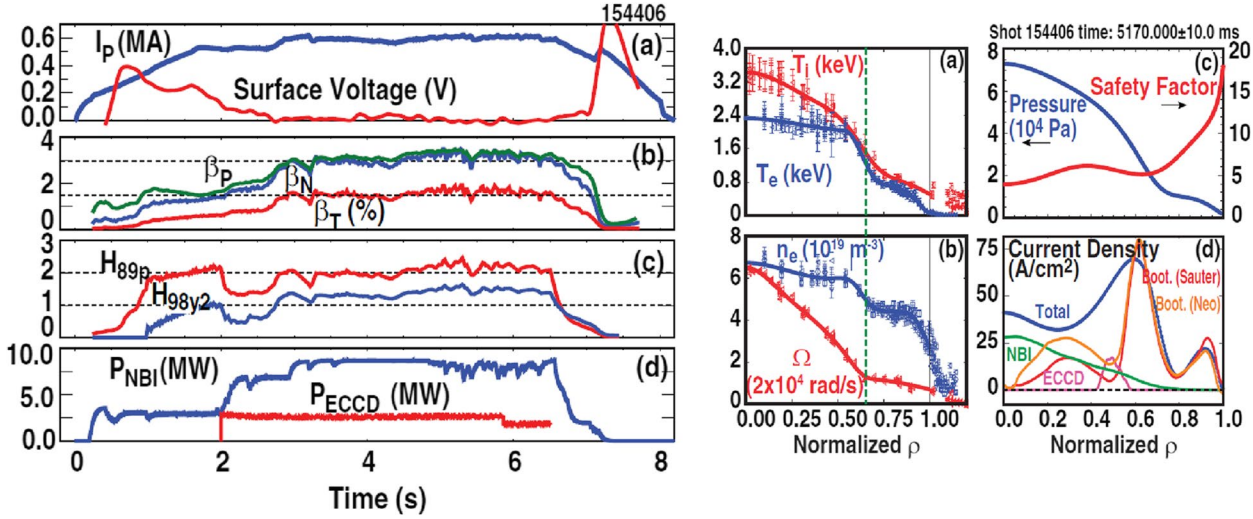

Fig. 2 Overview of high β_p discharge in DIIID (shot 154406) (Figures 1, 3 in [19])

the ETB region. It contributes the fully non-inductive current drive ($f_{BS} > 0.8$) with some contributions from NBI and EC current drive. There was no strong impurity accumulation observed. High β_N and β_p have been achieved with improvement of wall stabilization by expanding ITB foot and reducing the outer gap between the plasma and the wall. In these plasmas, it was revealed that the Shafranov shift effect strongly contributes to the confinement enhancement, and the higher performance can be sustained if Alfven eigenmode activity could be avoided by keeping $\nabla\beta_{fast}$ below $\nabla\beta_{fast,crit}$ so that fast-ion transport is reduced, where β_{fast} is the fast-ion beta.

2.2 Broad ITB without internal kink mode in HL-2A

In HL-2A, ITBs were formed with different MHD characteristics [11]. Three types were identified: ITB without internal kink mode, ITB with fishbone activity, and ITB with long-lived mode as presented in Fig. 3. It was turned out that ITB without internal kink mode has a weaker gradient than the ITB with fishbone and a smaller width than the ITB with long-lived mode. The ITB location is ρ_{ITB}~0.425 in the ITB without internal kind mode which is much larger than that of ITB with fishbone and with long-lived mode where ρ_{ITB}~0.172 and ~0.18, respectively. The line-averaged density of the ITB without internal kind mode is $2.1 \times 10^{19}\ m^{-3}$ much higher than that of ITBs with fishbone and long-lived mode.

2.3 F-ATB (fast ion-induced anomalous transport barrier) in ASDEX Upgrade

A new type of ITB was discovered in ASDEX Upgrade, the so-called F-ATB [25] as presented in Fig. 4. It is

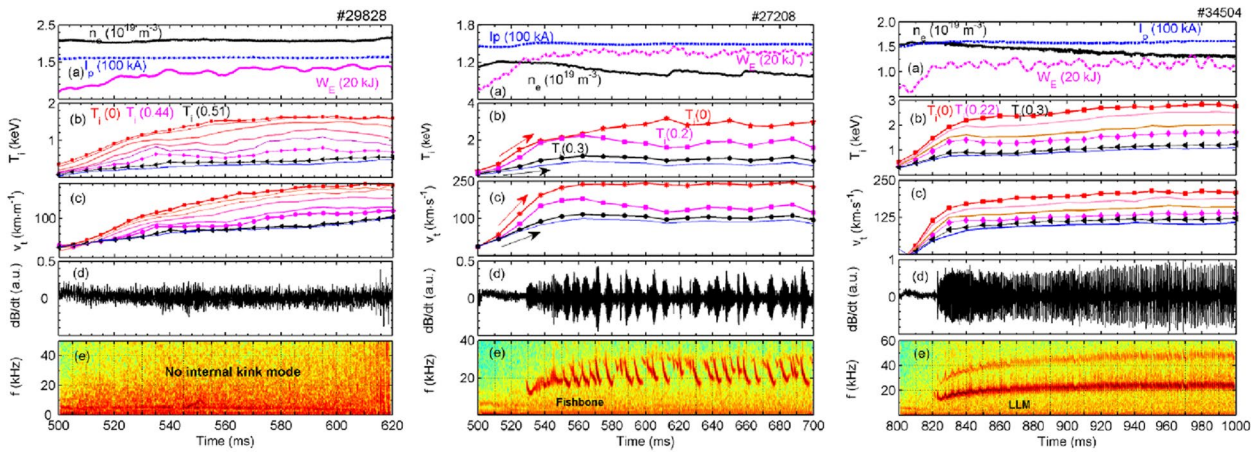

Fig. 3 ITB without internal kink mode, ITB with fishbone activity, and ITB with long-lived mode in HL-2A (Figures 15, 2, 3 in [11])

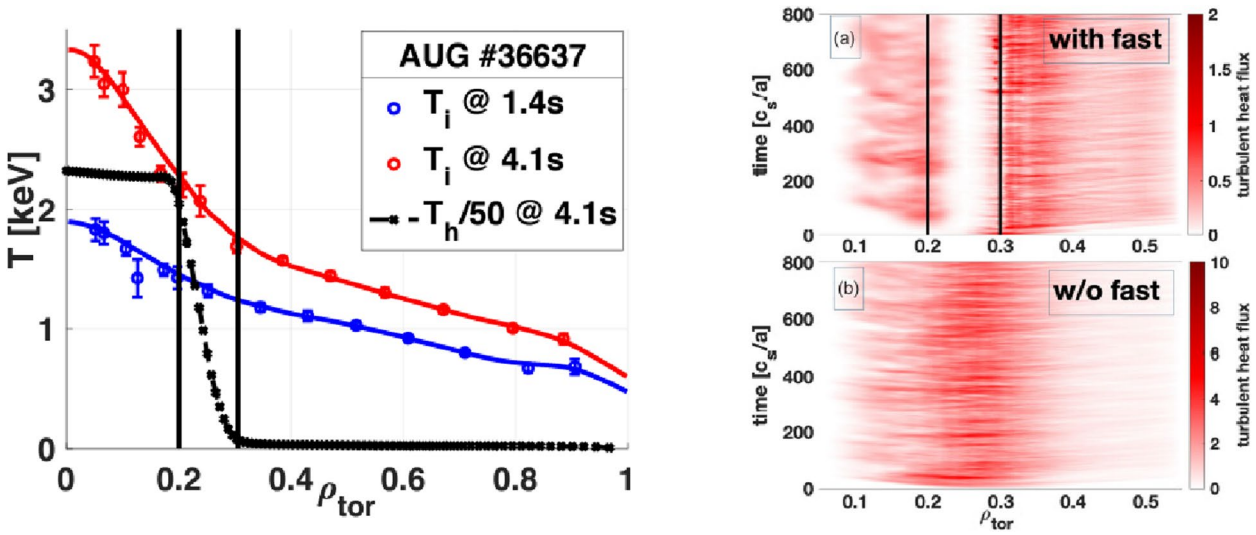

Fig. 4 (Left) main ion temperature profiles (T_i) at t =1.4 (blue) and t = 4.1 s (red) and equivalent fast-ion temperature of distribution function of the hydrogen minority (T_h rescaled by a factor of 50) at t = 4.1 s (black). The vertical black lines denote the region where the logarithmic temperature gradients deviate the most (Figure 1f in [25]). (Right) time evolution of the radial profile of the total ion heat flux (thermal ions þ hydrogen) in gyroBohm units. The same magnetic equilibrium and kinetic bulk profiles are employed in the simulations with (**a**) and without (**b**) the suprathermal ions (Figure 2a, b in [25])

characterized by a full suppression of the turbulent transport resulting from strongly sheared, axisymmetric E × B flows and an increase of the neoclassical counterpart, albeit keeping the overall fluxes at significantly reduced levels. The trigger mechanism is found to be a resonance interaction between suprathermal particles or fast ions which were generated via ion cyclotron resonance heating (ICRH) and ITG microturbulence, whose overall effect is the formation of localized layers in the E × B velocity and thus to ITB. It was demonstrated via global gyrokinetic simulations with GENE [26, 27] with realistic ion-to-electron mass ratio, collisions, and fast ions modeled with realistic background distributions which captured the formation of an ITB retaining all of these physical effects at once as shown in Fig. 4.

2.4 Ion and electron ITB in LHD

ITB has been observed in stellarators as well as tokamaks such as LHD [28–30], CHS [31], TJ-II [32], and W7-AS [33]. In LHD, ITBs have been obtained in the ion and the electron energy channel together as shown in Fig. 5d [34]. The central ion temperature was increased, while wall recycling was reduced. It was found that the peaking of the ion heating profile and the reduction of charge exchange

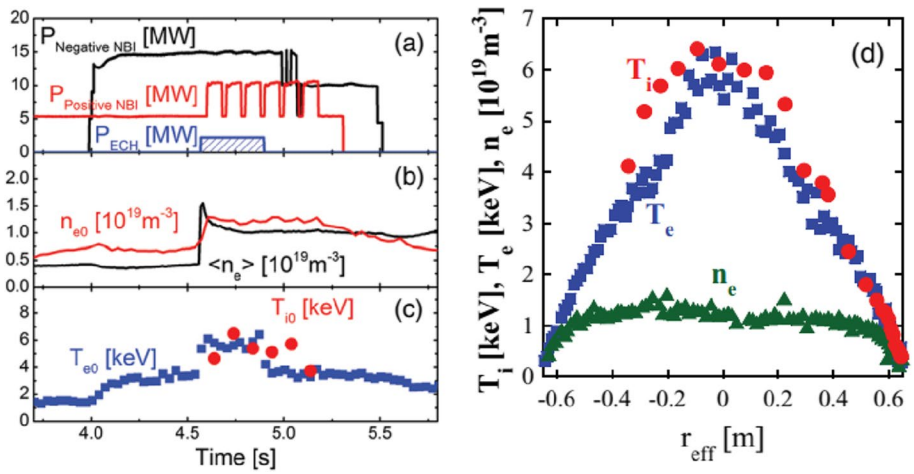

Fig. 5 Time evolution of main parameters of ion and electron ITB discharge in LHD (**a**), (**b**), (**c**) and ion and electron temperature and electron density profile (**d**) (Figure 5 in [34])

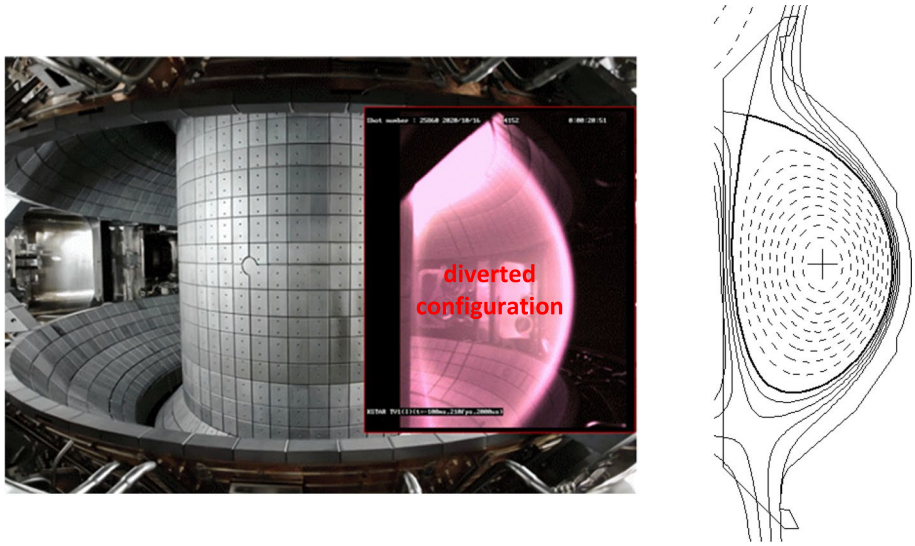

Fig. 6 **a** Camera image of KSTAR FIRE mode #25860. **b** Plasma configuration at 20 s of #25860

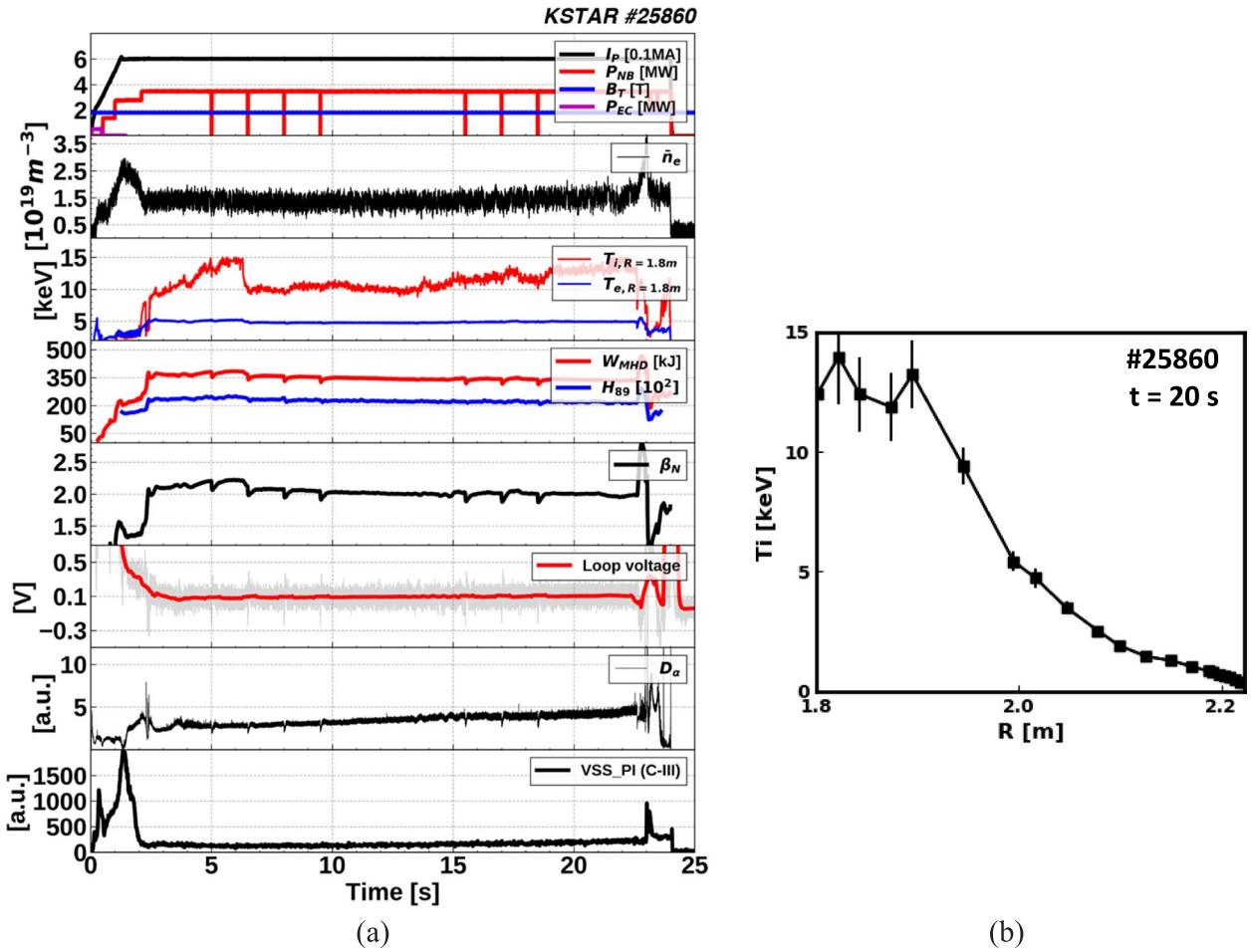

Fig. 7 **a** Overview of main parameters of KSTAR FIRE mode #25860; plasma current, NBI heating power, toroidal magnetic field strength, EC heating power, line-averaged electron density, central ion and electron temperature, total stored plasma energy, H_{89}, β_N, loop voltage, D_α, carbon-III impurity line radiation. **b** Ion temperature profile in radius at 20 s of #25860

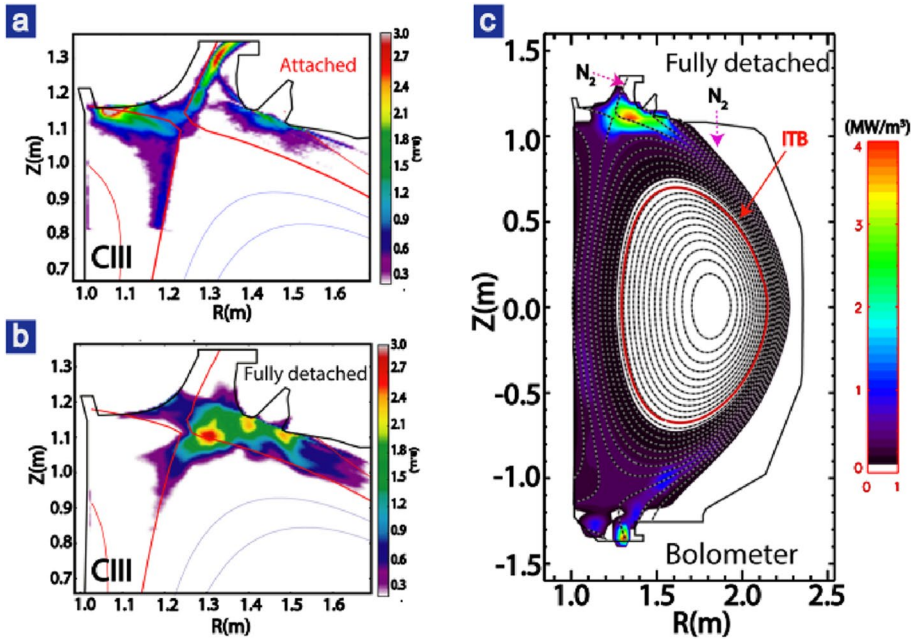

Fig. 8 2D radiation measured by bolometer (right) and CIII radiation from tangential TV (left) (Figure 3 in [39])

loss of energetic ions play an important role for further improvement of the ITB core. The electron ITB has been integrated with the ion ITB by applying ECH. The plasma density was kept low with the central value around 10^{19} m^{-3}.

2.5 FIRE (fast ion regulated enhancement) mode in KSTAR

A new stationary ITB discharge has been developed with a diverted configuration at q_{95} ~4–5 on KSTAR. It is noteworthy that typical ITB discharges have been obtained with limited configurations [14, 15]. A key to establish these discharges is to keep low plasma density so to avoid from L-mode to H-mode transition. In this aspect, the upper single null configuration with unfavorable B drift direction is more reliable to sustain this regime though this scenario can be obtained with both upper single null and lower single null configurations. As fast ions turned out to have significant roles in this new regime, it is coined as fast-ion-regulated enhancement mode [35].

Figure 6 shows a representative FIRE mode discharge in KSTAR, #25860. Figure 6a shows the image of a plasma confined in the KSTAR device. The plasma is in a divertor configuration with upper single null as shown in Fig. 6b.

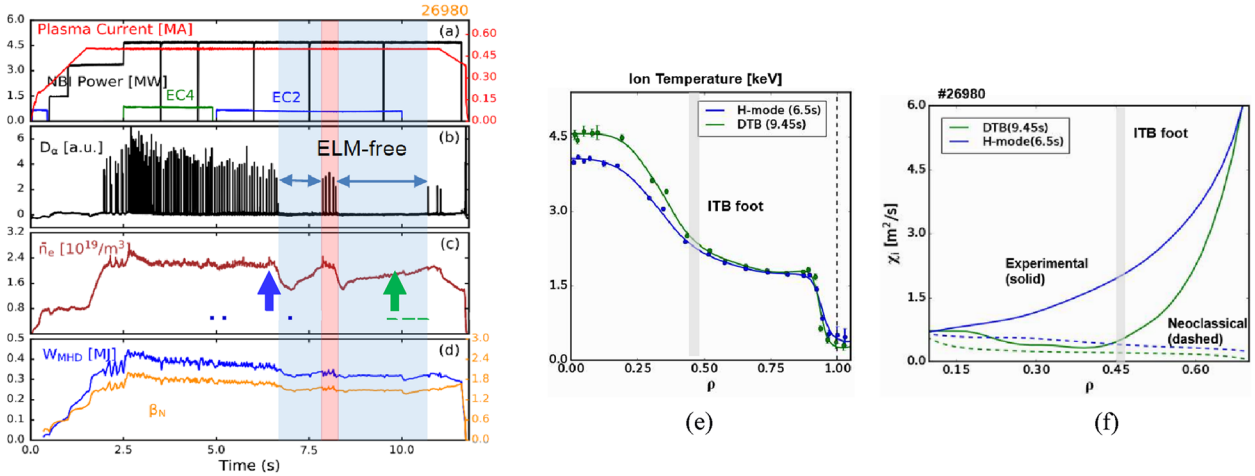

Fig. 9 Overview of a DTB discharge in KSTAR (**a**)–(**d**), ion temperature profiles (**e**), and ion heat diffusivity (**f**)

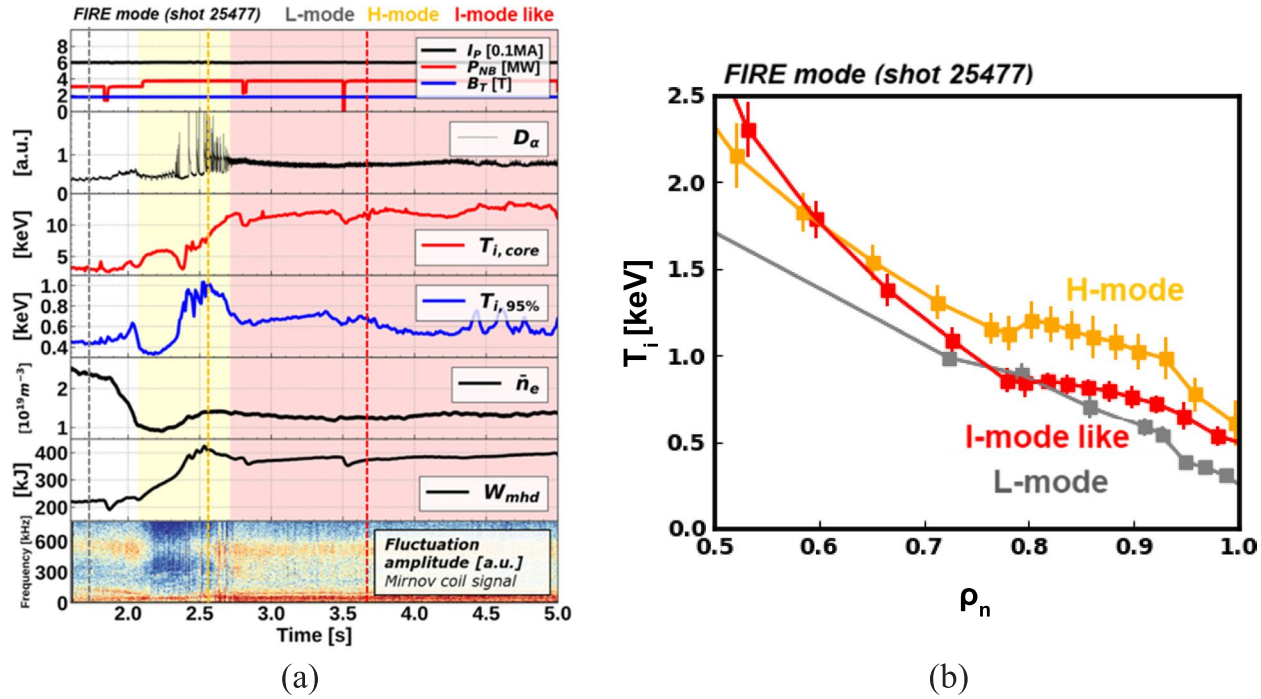

Fig. 10 **a** A FIRE mode discharge with I-mode like edge. **b** Comparison of the ion temperature profile between L-mode, H-mode, and I-mode like FIRE mode

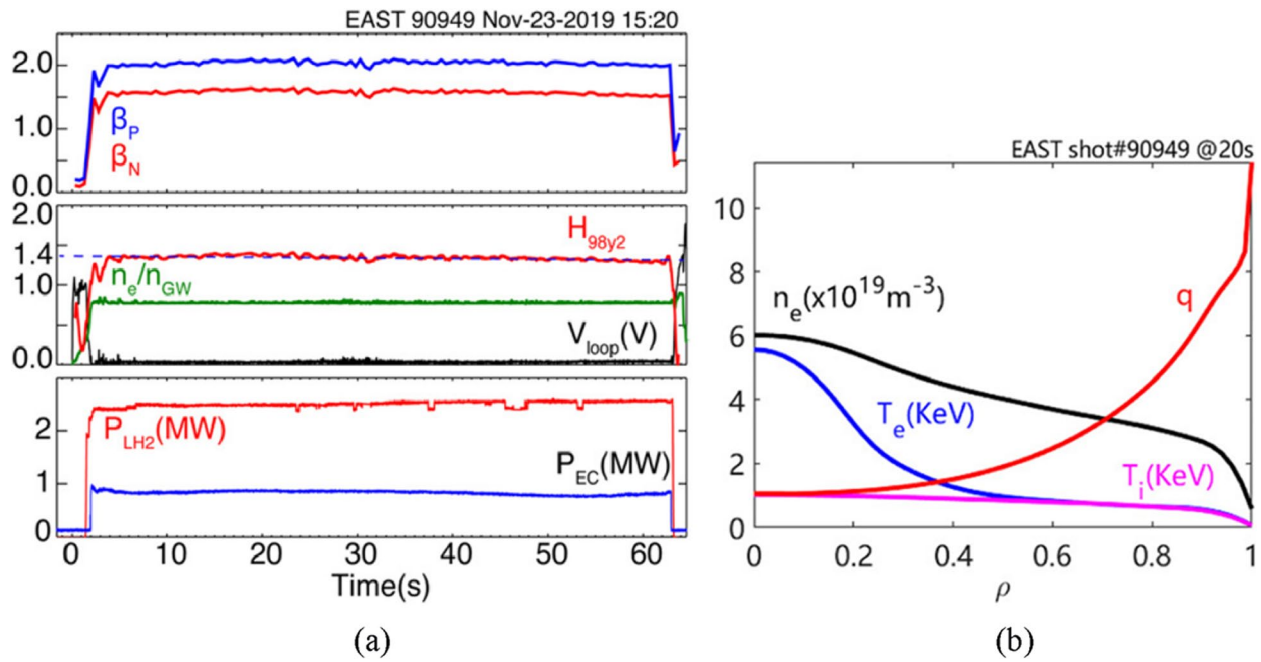

Fig. 11 **a** Time histories of several parameters for EAST 60 s high β_P long-pulse discharge. **b** Ion and electron temperature, electron density, and q-profile (Figures 1 and 2 from [43])

The main parameters are presented in Fig. 7. The plasma current is 0.6 MA, and the toroidal magnetic field strength is 2.0 T. About 4 MW of NBI power was applied for the purpose of ion heating mainly. The blips in NBI are for measurements of the toroidal rotation as well as the ion temperature by charge exchange recombination spectroscopy. The line-averaged density is kept constant around 1.5 $\times 10^{19}$ m^{-3}. The central ion temperature reached ~15 keV, but a quasi-coherent MHD activity caused reducing it to ~10 keV. But its impact to the total plasma energy is little because the affected area is small owing to its localization in the central region. β_N and H_{89} were sustained about 2.0 in the entire flattop phase of the plasma current, where H_{89} is the energy confinement enhancement factor based on L-mode scaling corresponding to ~$0.5H_{98}$. It is noteworthy that the performance of FIRE modes could be similar to that of hybrid modes [36]. The loop voltage was around 0.1 V which is very low level compared to conventional H-modes in KSTAR implying close to fully non-inductive current drive. It is noteworthy that FIRE mode discharges usually exhibit the loop voltage below 0.1 V. As shown in D_α, there were no harmful ELM activities. The stationary carbon-III impurity line radiation presents that there are no severe impurity accumulations in this discharge. It is noteworthy that other radiation or effective charge (Z_{eff}) measurements are currently limited in KSTAR. However, this low impurity accumulation can be supported by a constant central electron temperature. Note that the central electron temperature drops so that flat or hollow electron temperature profiles can be observed while with severe impurity accumulations in the core region. The ion temperature profile at 20 s is shown in Fig. 7b. It exhibits a weak, large, and wide ITB characteristics. The FIRE mode discharges are very stable where no severely harmful instabilities are present. The internal inductance, l_i, is high so that beta limit is inherently high. If transition to H-mode is avoided, ITB can be sustained without any delicate feedback control such as kinetic profile controls.

The effect of the fast ion to the confinement enhancement was evaluated by linear and nonlinear gyrokinetic

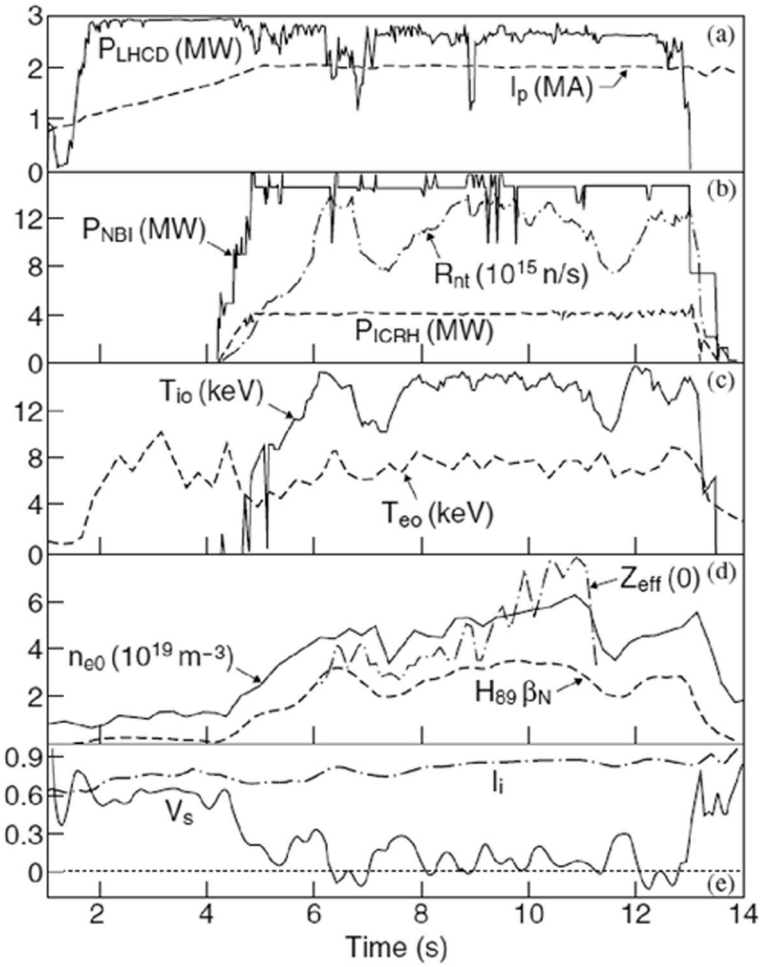

Fig. 12 Overview of quasi-stationary ITB with active control of p(r) in JET (shot 53521) (Figure 1 from [46])

simulations at $\rho_{tor} = 0.4$ and $t = 5.35$ s for KSTAR FIRE mode discharge #22663. The linear simulations with GKW [37] showed that the electromagnetic stabilization effect can be reinforced by fast ions. The Shafranov shift effect, the so-called α-effect, can also be reinforced by fast ions. Most significantly, the dilution of the thermal ions and subsequent reduction in the normalized density gradient length, R/L_n, were found to suppress the ITG turbulence. Local nonlinear simulations were conducted with CGYRO [38]. It was revealed that the fast ions significantly reduce thermal energy flux, confirming the role of fast ions for energy confinement enhancement.

3 Core-edge integration in ITB discharges

3.1 High β_p plasmas in DIII-D

Operations with high Greenwald density fraction of ~90% were achieved without degradation of plasma performance with divertor detachment in high β_p plasmas in DIII-D as shown in Fig. 8 [39]. The good energy confinement of H_{98} ~1.5 was sustained with the full divertor detachment that is the first time in a tokamak. It was revealed that although the pedestal pressure degraded due to detachment, the high β_p scenario facilitates divertor detachment which, in turn, promotes the development of an even stronger ITB at large radius with a weaker ETB. This self-organized synergy between ITB and ETB leads to a net gain in energy confinement, in contrast to the net confinement loss caused by divertor detachment in standard H-modes.

3.2 Double transport barrier without ELMs in KSTAR

Stationary double transport barriers (DTB) without ELM were formed with density drop and sustained about 3 s [40]. The ion thermal transport is reduced to the neoclassical level inside the ITB foot during the DTB phase as

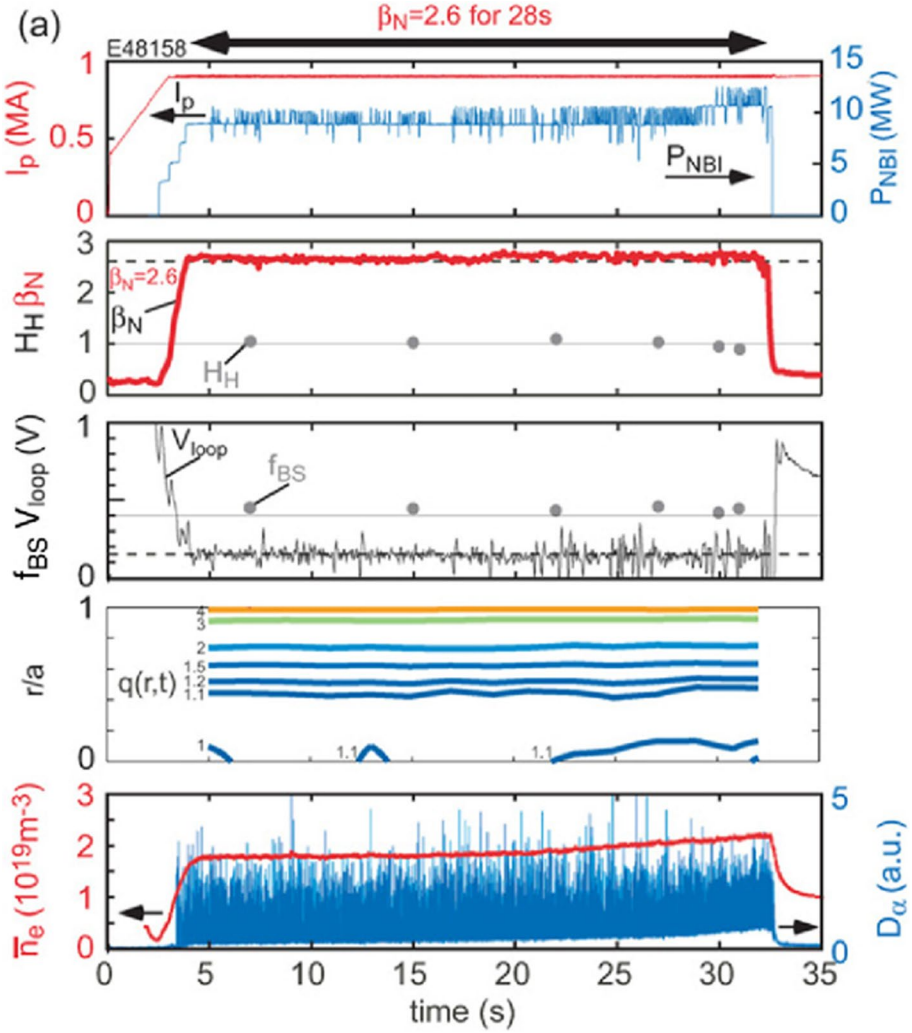

Fig. 13 Overview of long-pulse hybrid mode in JT-60U (shot 48158) (Figure 1 from [47])

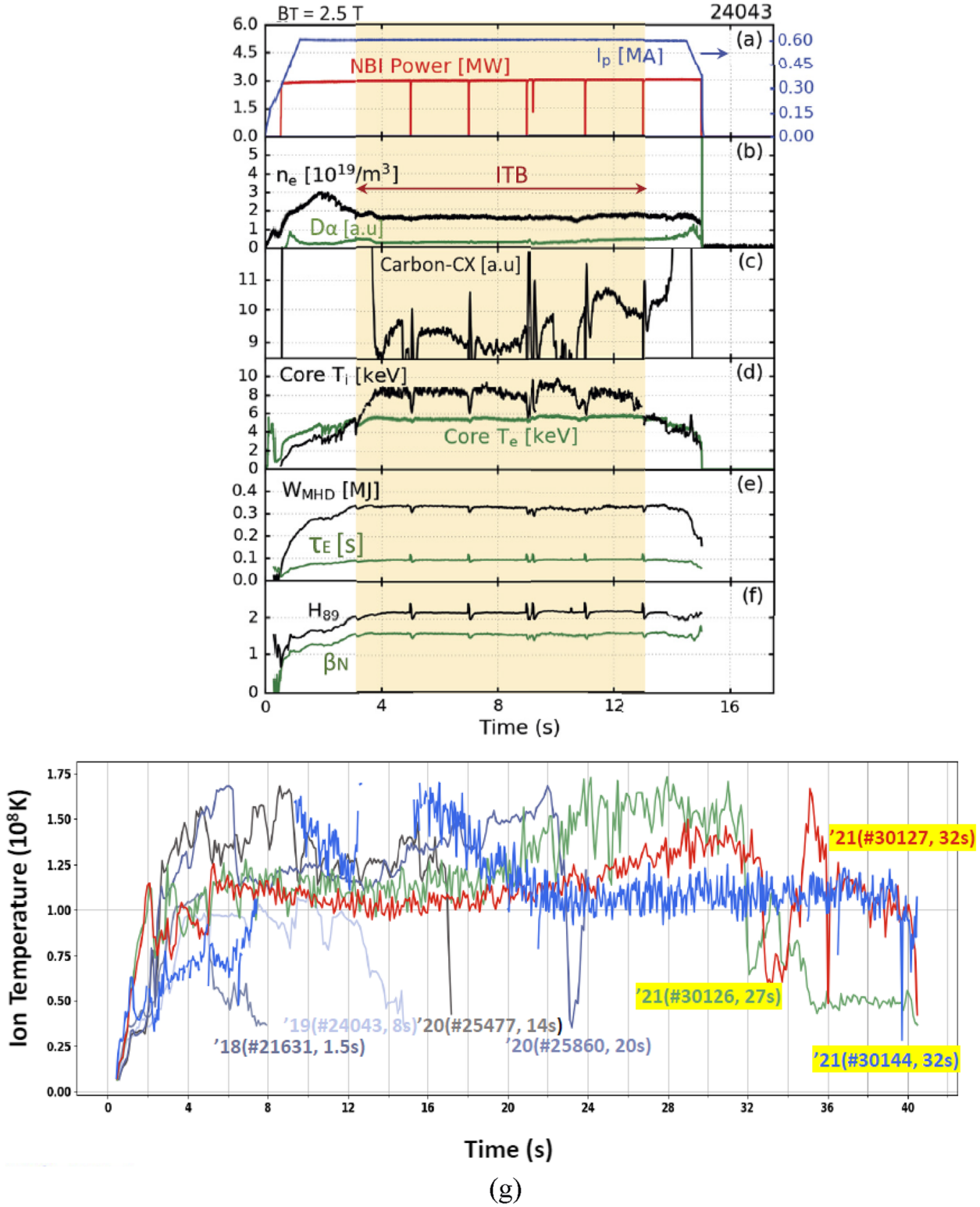

Fig. 14 **a**–**f** Time evolution of long-pulse ITB discharge at KSTAR (shot 24043) (Figure 8 from [15]). **g** Progress of sustainment of high ion temperature in long-pulse operations with ITB in KSTAR

shown in Fig. 9f. ELM-free is thought to be originated from the reduced pressure gradient. Further investigation of double transport barrier formation is in progress.

3.3 FIRE-mode with I-mode-like edge in KSTAR

Some of FIRE modes are equipped with ETB formed only in the energy channel not in the particle channel like I-mode as shown in Fig. 10a [35]. They show a high ion temperature gradient at the edge region, higher than that of L-mode as presented in Fig. 10b and no clear barrier in the density profile as in I-modes [41, 42]. The absence of the particle transport barrier can enhance the fraction of fast ions by reducing thermalization of fast ions with a low density. The presence of energy ETB contributes to increase the performance of FIRE mode and also increase the bootstrap current fraction.

4 Long sustainment of ITBs

4.1 Long pulse with electron ITB mode in EAST

A recent EAST experiment has successfully demonstrated long-pulse steady-state high plasma performance scenario [43–45]. A discharge with a duration over 60 s with β_P~2.0, β_N~1.6, and H_{98}~1.3 and an ITB on the electron energy channel is obtained with EC and lower hybrid (LH) heating and current drive as shown in Fig. 11. A higher β_N (β_N~1.8, β_p~2.0, H_{98y2}~1.3, n_e/n_{GW}~0.75) with a duration of 20 s is achieved by using the modulated NBI and multi-RF power. The high-Z impurity accumulation in the plasma core is well controlled in a low level by using the on-axis ECH. The m/n=1/1 mode can interact with small-scale turbulence, which is driven by electron temperature gradient, hence reduce the turbulence amplitude. The central values of q-profile can be controlled around unity to stabilize the sawtooth instabilities; otherwise, the sawtooth instabilities will reduce performance and might trigger deleterious instabilities.

4.2 Quasi-stationary ITB with active control of p(r) in JET

Quasi-stationary operation has been achieved with the discharge time limited only by plant constraints (B_t flattop) [46]. Full current drive was obtained over all the high-performance phase by using LHCD at q_{95} < 6.5 as shown in Fig. 12. Feedback control on the total pressure and on the electron temperature profile was implemented by using, respectively, NBI and ICRH. Impurity accumulation appeared but partly controlled by applying ICRH.

4.3 High β_p mode (hybrid mode) in JT-60U

Hybrid scenarios based on high β_p ELMy H-mode plasmas have been established with weak ITBs at I_P = 900 kA, B_T = 1.54 T, and q_{95}~3.2 which was sustained for 28 s [47]. High performance of β_N > 2.6 and $H_{98} \geq 1$ with f_{BS} = 0.43 was maintained as shown in Fig. 13. There was no NTMs, but infrequent sawtooth and n = 1 mode were observed. During the discharge, the confinement was gradually degraded due to wall recycling which can be seen in Fig. 13, where the density and D_α were increased, while the NBI beam power was increased to keep the performance constant.

4.4 Conventional ITB and FIRE mode in KSTAR

Stable conventional ITBs were achieved with the plasma shape control in marginally limited plasma (upper single null like) in KSTAR. Performance close to standard H-modes of β_N~1.6 and H_{89L}~2.2 was sustained about 10 s. The central ion temperature was $T_{i,0}$~9 keV. The control of striking point was essential to minimize the inflow of impurities for long-pulse discharges [15]. FIRE mode was sustained up to 30 s with $T_{i,0}$~9 keV. The progress of long-pulse operation with conventional ITB and FIRE mode is presented in Fig. 14 and Table 1.

5 Conclusions

To achieve the goal of tokamak plasma research, (i) high fusion performance, (ii) steady-state operation, and (iii) long-pulse operation, ITB experiments have been actively conducted in various tokamak devices. Significant progress has been made recently such as in high β_p plasmas in DIII-D, broad ITB without internal kink mode in HL-2A, F-ATB in ASDEX Upgrade, ion and election ITB in LHD, FIRE mode, and DTB in KSTAR. Outstanding progress has also been achieved in long sustainment of ITB in high β_p mode with electron ITB in EAST, quasi-stationary ITB with active control of pressure profile in JET, hybrid mode with weak ITBs in JT-60U, and stationary ITB and FIRE mode in KSTAR.

There are still challenges remaining for ITB discharges to become a reliable and robust scenario for a fusion reactor. For reliable core-edge integration, understanding the particle transport is essential [48]. Weak and small ITBs without ETB require further current drive for steady-state operations. Utilizing self-generated current [49–52] in addition to bootstrap current would be desirable. Long

Table 1 Progress of sustainment of high ion temperature in long-pulse operations with ITB in KSTAR

	`16	`17	`18	`19	`20	`21	`22
NB power	~ 5 MW		~ 3 MW		3 ~ 4 MW		
High-T_i (> 10^8 K) duration	-		< 15 s		~ 30 s		
Shape	Limited		USN-like limited		USN diverted		

sustainment of ITBs, at least in the ion energy channel, over the wall saturation time by incorporating high performance with high density in steady-state conditions would be the most promising way for ITB scenarios using thermonuclear fusion. Relying on beam-target fusion in fast-ion rich plasmas such as in FIRE mode can be chased as an alternative approach, for example, in reactors using proton-boron species.

Acknowledgements
The author gratefully acknowledges the Research Institute of Energy and Resources and the Institute of Engineering Research at Seoul National University.

Funding
This work was supported by the National R&D Program through the National Research Foundation of Korea (NRF) funded by the Korea government (Ministry of Science and ICT) (NRF-2021M1A7A4091135).

Availability of data and materials
The data that support the plots within this paper and other findings of this study are available from the corresponding author upon reasonable request.

Declarations

Ethics approval and consent to participate
Not applicable

Competing interests
The author declares no competing interests.

Received: 17 September 2023 Accepted: 10 November 2023
Published online: 21 November 2023

References

1. M. Shimada et al., Nucl. Fusion **47**, S1 (2007)
2. F. Wagner et al., Phys. Rev. Lett. **49**, 1408 (1982)
3. W.M. Nevins et al., IAEA Fusion Energy Conference (1992).
4. Y. Koide et al., Phys. Rev. Lett. **72**, 3662 (1994)
5. D.R. Ernst et al., Phys. Plasmas **11**, 2637 (2004)
6. K. Zhurovich et al., Nucl. Fusion **47**, 1220 (2007)
7. O. Gruber et al., Plasma Phys. Controlled Fusion **42**, A117 (2000)
8. G. Tardini et al., Nucl. Fusion **47**, 280 (2007)
9. B.W. Rice et al., Phys. Plasmas **3**, 1983 (1996)
10. S. Ding et al., Phys. Plasmas **24**, 056114 (2017)
11. X.X. He et al., Plasma Phys. Controlled Fusion **64**, 015007 (2022)
12. C. Gormezano, Plasma Phys. Controlled Fusion **41**, B367 (1999)
13. T. Fujita et al., Phys. Rev. Lett. **78**, 2377 (1997)
14. J. Chung et al., Nucl. Fusion **58**, 016019 (2018)
15. J. Chung et al., Nucl. Fusion **61**, 126051 (2021)
16. F.M. Levinton et al., Phys. Rev. Lett. **75**, 4417 (1995)
17. X. Litaudon et al., Plasma Phys. Controlled Fusion **41**, A733 (1999)
18. K. Ida, T. Fujita, Plasma Phys. Controlled Fusion **60**, 033001 (2018)
19. A.M. Garofalo et al., Nucl. Fusion **55**, 123025 (2015)
20. M. Kikuchi, Nucl Fusion **30**, 265 (1990)
21. J. Candy et al., Phys. Plasmas **16**, 060704 (2009)
22. G.M. Staebler et al., Phys. Plasmas **14**, 055909 (2007)
23. A. Bellie, J. Candy, Plasma Phys. Control. Fusion **50**, 095010 (2008)
24. S. Ding, A. Garofalo, Reviews of Modern Plasma Physics **7**, 4 (2023)
25. A. Di Siena, A. et al., Phys. Rev. Lett. **127**, 025002 (2021).
26. F. Jenko et al., Phys. Plasmas **7**, 1904 (2000)
27. T. Görler et al., J. Comput. Phys. **230**, 7053 (2011)
28. K. Ida et al., Phys. Rev. Lett. **91**, 085003 (2003)
29. N. Kenmochi et al., Sci. Rep. **10**, 5 (2020)
30. N. Kenmochi et al., Sci. Rep. **12**, 6979 (2022)
31. A. Fujisawa et al., Phys. Rev. Lett. **82**, 2669 (1999)
32. F. Castejón et al., Nucl. Fusion **42**, 271 (2002)
33. U. Stroth et al., Phys. Rev. Lett. **86**, 5910 (2001)
34. K. Nagaoka et al., Nucl. Fusion **55**, 113020 (2015)
35. H. Han, S.J. Park, Y.-S. Na, et al., Nature **609**, 269 (2022)
36. Y.-S. Na et al., Nucl. Fusion **60**, 086006 (2020)
37. A.G. Peeters et al., Comput. Phys. Commun. **180**, 2650 (2009)
38. J. Candy, E.A. Belli, R.V. Bravenec, J. Comput. Phys. **324**, 73 (2016)
39. L. Wang et al., Nature Comm. **12**, 1365 (2021)
40. Lee, M. W. et al., Observation of stationary double transport barriers in KSTAR, IAEA Fusion Energy Conference Proceeding, EX/P2-8 (2023).
41. R.M. McDermott et al., Phys. Plasmas **16**, 056103 (2009)
42. Z.X. Liu et al., Phys. Plasmas **23**, 120703 (2016)
43. X.Z. Gong et al., Nucl. Fusion **62**, 076009 (2022)
44. H. Jiansheng et al., AAPPS Bull. **33**, 8 (2023)
45. G.S. Xu et al., AAPPS Bull. **23**(1), 9–13 (2013)
46. F. Crisanti et al., Phys. Rev. Lett. **88**, 145004 (2002)
47. N. Oyama et al., Nucl. Fusion **49**, 104007 (2009)
48. Y.-S. Na et al., Nucl. Fusion **59**, 076026 (2019)
49. W. Wang et al., Nucl. Fusion **59**, 084002 (2019)
50. S. Yi et al., Phys. Plasmas **23**, 102514 (2016)
51. E. Li et al., Phys. Rev. Lett. **128**, 085003 (2022)
52. Y.-S. Na, J. Seo, et al., Nature Comm. **13**, 6477 (2022)

Publisher's Note